

Relevant Interactions of Antimicrobial Iron Chelators and Membrane Models Revealed by Nuclear Magnetic Resonance and Molecular Dynamics Simulations

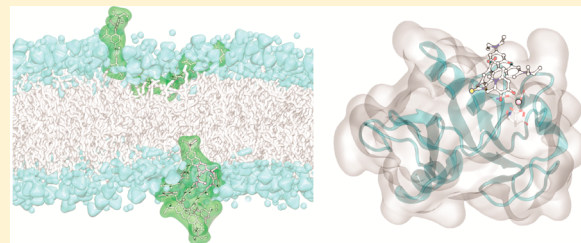
João T. S. Coimbra,^{†,§} Tânia Moniz,^{†,§} Natércia F. Brás,^{†,§} Galya Ivanova,^{†,§} Pedro A. Fernandes,[†] Maria J. Ramos,^{*,†} and Maria Rangel^{*,‡}

[†]REQUIMTE, Departamento de Química e Bioquímica, Faculdade de Ciências, Universidade do Porto, Rua do Campo Alegre s/n, 4169-007 Porto, Portugal

[‡]REQUIMTE, Instituto de Ciências Biomédicas de Abel Salazar, Universidade do Porto, Rua Jorge Viterbo Ferreira, 228, 4050-313, Porto, Portugal

Supporting Information

ABSTRACT: The dynamics and interaction of 3-hydroxy-4-pyridinone fluorescent iron chelators, exhibiting antimicrobial properties, with biological membranes were evaluated through NMR and molecular dynamics simulations. Both NMR and MD simulation results support a strong interaction of the chelators with the lipid bilayers that seems to be strengthened for the rhodamine containing compounds, in particular for compounds that include ethyl groups and a thiourea link. For the latter type of compounds the interaction reaches the hydrophobic core of the lipid bilayer. The molecular docking and MD simulations performed for the potential interaction of the chelators with DC-SIGN receptors provide valuable information regarding the cellular uptake of these compounds since the results show that the fluorophore fragment of the molecular framework is essential for an efficient binding. Putting together our previous and present results, we put forward the hypothesis that all the studied fluorescent chelators have access to the cell, their uptake occurs through different pathways and their permeation properties correlate with a better access to the cell and its compartments and, consequently, with the chelators antimicrobial properties.



INTRODUCTION

Our group has been working on the design of iron chelators that may be of use in new strategies to fight infection based on the concept of iron deprivation. Chelators were prepared by conjugating 3-hydroxy-4-pyridinone chelating units with xanthene fluorophores in order to provide compounds with distinct fluorescence emission spectrum, hydrophilic/lipophilic balance and charge at physiological pH (Figure 1).

Evaluation of the effect of chelators in a *Mycobacterium avium* infection model proved that the compounds limit the access of iron to bacteria and have a significant inhibitory effect in the intramacrophagic growth of *M. avium* bacteria.^{1–3} The results showed that (i) the activity of the chelators is strongly dependent on the presence of the fluorophore on the molecular framework and (ii) the inhibitory effect of the rhodamine B isothiocyanate derivatives (MRH7=CP777=4 and MRB7) is superior to those observed for carboxytetramethylrhodamine chelators (MRH8 and MRB8) and fluorescein chelators (MRH5=CP852).

Results of comparative studies of the partition of the compounds and distribution of the compounds, obtained from fluorescence spectroscopy and confocal microscopy, provide evidence that the biologically active compounds strongly interact with lipid phases and remain largely membrane

bound while the less-active do not.³ Moreover, the results suggest that a surface effect is quite important for the interaction with the membrane as reported for rhodamine B conjugated peptides.^{4,5} Considering the latter results, we hypothesized that rhodamine B potentiates the effect of the iron chelator by targeting the phagosomal membrane and by tethering the chelator to it, thus allowing successful competition with mycobacterial siderophores.

Considering that the permeation process of drugs across a lipid bilayer is crucial to understand the mechanism of drug action and a significant contribution to the development of new bioactive molecules we further explore, in the present work, the dynamics and interaction of the synthesized iron chelators with lipid bilayers by Nuclear Magnetic Resonance (NMR) and Molecular Dynamics simulations in order to substantiate our former premise.

Moreover, our previous confocal microscopy data show that the chelators go into macrophages but no detailed information regarding their pathways or mechanism of entrance has been obtained yet. Considering the chelators large size and the fact

Received: September 19, 2014

Revised: November 18, 2014

Published: December 1, 2014



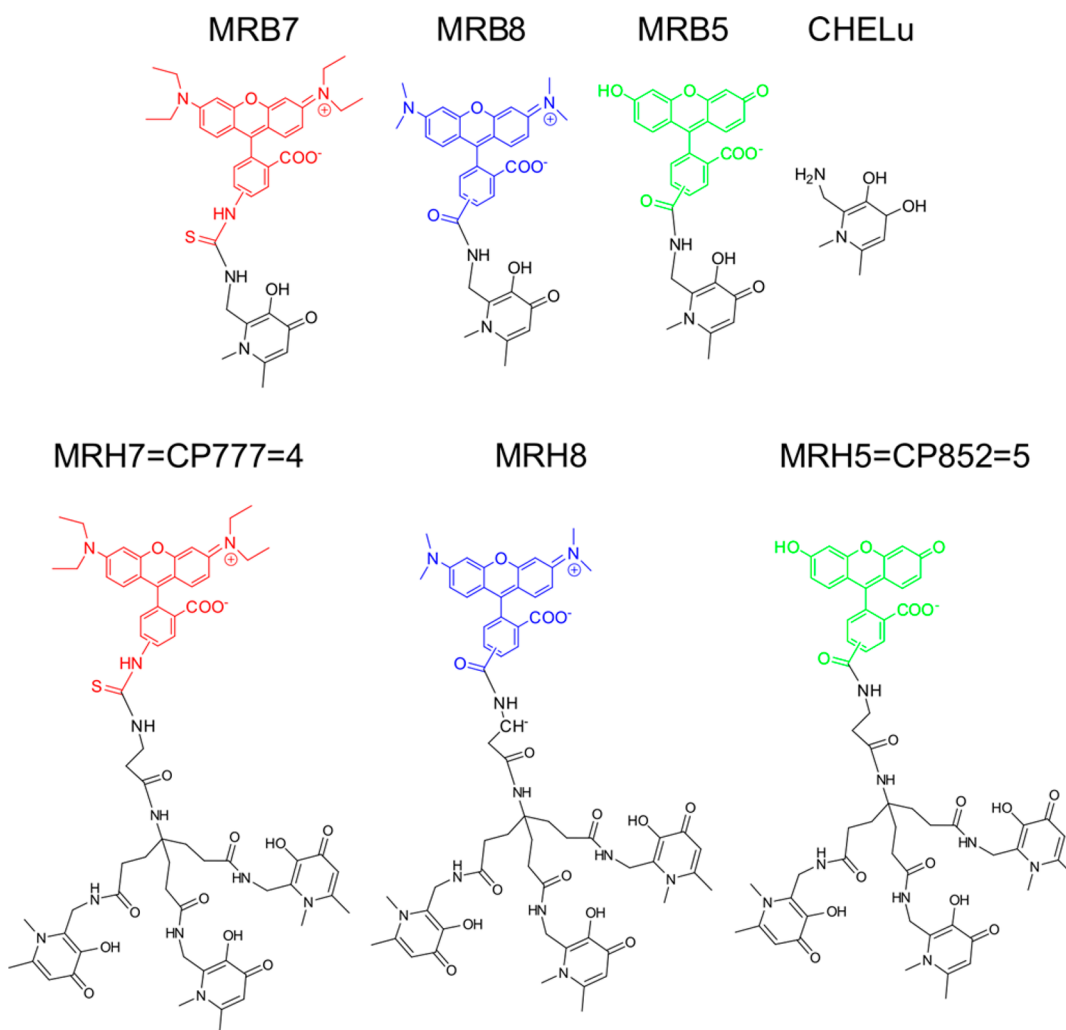


Figure 1. Formulas and abbreviation of 3-hydroxy-4-pyridinone chelators.

that many ligands and glyco-conjugated molecules access cells via transmembrane receptors, this could be an acceptable way for the internalization of the analyzed compounds. Both mannose and DC-SIGN (dendritic cell-specific intercellular adhesion molecule-3-grabbing nonintegrin) receptors exist on macrophages and they may be involved in the recognition of *Mycobacterium tuberculosis*.^{6,7} DC-SIGN receptors on the surface of macrophages recognize and bind to mannose-type carbohydrates or mannose analogous compounds commonly found on viruses, bacteria and fungi. Moreover, this binding is mediated by the presence of Ca^{2+} cations. It has also been suggested that the mechanism for endosomal release is mediated by auxiliary calcium, which serves as a pH sensor. Acidic pH induces a removal of Ca^{2+} that results in conformational rearrangements of the receptor, turning it unable to bind compounds.^{6,7}

Although we found no experimental data supporting this choice of receptor, the type of cells that are targeted and the highly ringed structure of the compounds have prompted us to choose this mannose-binding protein. Hence, to evaluate the binding of the MRB7, MRB8, and MRB5 compounds, several molecular docking and molecular dynamics (MD) simulations were performed.

■ EXPERIMENTAL METHODS

Materials. Chemicals were obtained from Sigma-Aldrich (grade puriss, p.a.) and were used as received unless otherwise specified. The lipid 1,2-dimyristoyl-sn-glycero-3-phosphocholine (DMPC) was purchased from Avanti Polar Lipids (Alabaster, AL).

Methods. Liposome Preparation. DMPC liposomes were prepared by evaporation to dryness, using a stream of nitrogen, of a lipid solution in chloroform. The film was maintained under vacuum, for a minimum of 4 h, to remove all traces of the organic solvent. The resulting dried lipid film was dispersed with D_2O (≈ 20 mM) and the mixture was vortexed above the phase-transition temperature ($37 \pm 0.1^\circ\text{C}$) to produce multilamellar liposomes (MLVs). The multilamellar liposomes were then exposed to the following cycle five times: freeze vesicles in liquid nitrogen and thaw in a water bath at $37 \pm 0.1^\circ\text{C}$. Lipid suspensions were equilibrated at $37 \pm 0.1^\circ\text{C}$ for 30 min and extruded ten times through polycarbonate filters (100 nm) to produce large unilamellar vesicles (LUVs). Extrusion of liposomes was performed with a Lipex Biomembranes (Vancouver, Canada) extruder attached to a circulating water bath. The size distribution of extruded DMPC liposomes was determined by dynamic light scattering analysis using a Malvern Instruments Zetasizer nano ZS.

Chelator Stock Solutions and Chelator/Liposome Mixtures for NMR Analysis. Stock solutions of compounds MRB7 and MRB8 were obtained by preparing a 1.2 mM solution of the compound in dimethyl sulfoxide ($\text{DMSO}-d_6$). The DMPC liposome suspensions were degassed with a stream of nitrogen for 20 min prior to the addition of the chelator stock solution. For the preparation of NMR samples 15 μL of the chelator DMSO stock solution was added to the DMPC liposome suspension ($\approx 20 \text{ mM}$) to provide a final concentration of approximately 30 μM of chelator in the samples. The choice of this concentration and molecular ratio was based on the concentration of chelator used in the biological studies. After addition of the chelator solution to the liposome suspension, the mixtures were vigorously agitated for 5 min producing the samples labeled DMPC_MRB7 and DPMC_MRB8.

NMR Spectroscopy. All NMR experiments were recorded on a Bruker Avance III 600 HD spectrometer, operating at 600.13 MHz for ^1H , equipped with 5 mm CryoProbe Prodigy and pulse gradient units, capable of producing magnetic field pulsed gradients in the z -direction of 50 G cm^{-1} . The NMR measurements were carried out in deuterium oxide (D_2O), at 310 K and spectral width of 10000 Hz. ^1H NMR experiments were performed with water suppression using excitation sculpting with gradients.⁸ Chemical shifts of the ^1H NMR signals were obtained by referring to the absorption frequency of the solvent deuteron monitored as the lock signal and further scaled to the resonance frequency of dimethyl sulfoxide- d_6 ($\text{DMSO}-d_6$) added in equal amount (15 μL) to all samples.

Proton registered diffusion-ordered NMR (^1H DOSY) experiments were acquired using the bipolar longitudinal eddy current delay (BPPILED, bipolar pulsed field gradient longitudinal eddy delay) pulse sequence.⁹ The experimental conditions (5 mm NMR tubes, samples composition, chelators and liposome concentration, temperature, no sample rotation and air flow of 500 L h^{-1}) for all DOSY experiments were kept constant. Before starting the NMR experiments, the temperature was equilibrated and maintained at 310 K, as measured using the spectrometer thermocouple system. Typically, in each experiment a number of 16 spectra of 16K data points and 64 scans were collected, with values for the duration of the magnetic field pulse gradients (δ) of 4 ms, diffusion times (Δ) of 400 ms and an eddy current delay set to 5 ms. The pulse gradient (g) was incremented from 2 to 98% of the maximum gradient strength in a linear ramp. The spectra were processed with the Bruker Topspin software package (version 3.2). The diffusion coefficients (D) were determined from the resonance signals of the N -methyl protons of the choline residues of DMPC (γ in Figure 2) and were all scaled to the absolute D value obtained for $\text{DMSO}-d_6$ (15 μL /per sample; $1.73 \times 10^{-9} \text{ m}^2 \text{ s}^{-1}$, calculated standard deviation of 1.1×10^{-3}) used as an internal reference. For each of the chelators' samples at least three independent experiments were performed, using freshly prepared liposomes and acquisition of NMR spectra in the time interval from 30 min to 48 h upon addition of the chelators to the liposome solution.

THEORETICAL METHODS

Parameterization. A total of five molecules were parameterized: MRB5, MRB7, MRB8, MRH7, and the Fe^{3+} complex of MRH7 (MRH7: Fe^{3+}). RESP model charges¹⁰ of the compounds were obtained with HF/6-31G(d),^{11–18} consistent with the procedure employed in the general amber force field (GAFF).¹⁹ The charges were obtained from B3LYP/6-31G-

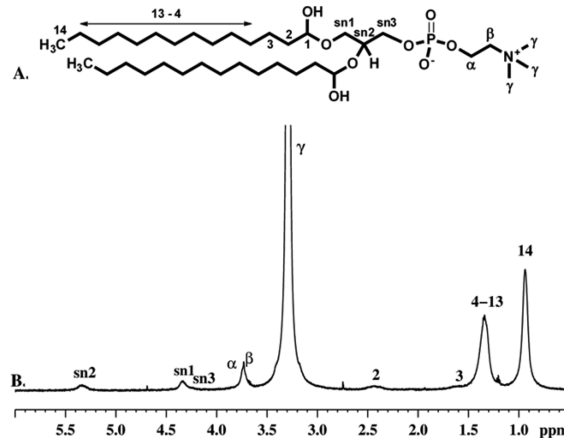


Figure 2. Formula of the lipid 1,2-dimyristoyl-sn-glycero-3-phosphocholine (DMPC) (A) and ^1H NMR spectrum of DMPC liposomes in D_2O at 310 K with the assignment of the characteristic proton resonances in the molecule (B).

(d)^{20–23} optimized structures. The GAFF atom types for our molecules were acquired through the ANTECHAMBER program.

Regarding MRH7: Fe^{3+} , we have followed a standard protocol for transition metal systems, already employed with success.^{24,25} Potential energy surface scans were performed for the bonds and angles comprising the metal coordinated atoms. Respective bond stretching and angle bending parameters were obtained with the B3LYP/6-31G(d):SDD combination (with the SDD pseudopotential basis set²⁶ applied only on the metal atom). RESP model charges were obtained with B3LYP/6-311+G(2d,2p).^{27–33} The obtained parameters are described in detail in the Supporting Information (see Table S1 and Figure S1). The van der Waals parameters for iron were obtained from the literature³⁴ and dihedral angles were set to 0.

Compounds: Membrane Interaction. An atomistic and dynamic view of the interaction of the compounds with biological membrane models is provided. For this purpose, a set of MD simulations were performed to evaluate the interaction of the studied compounds with a computational membrane model composed of the phospholipid DMPC and of TIP3P³⁵ water molecules. The systems were composed of 400 phospholipids (in a bilayer lamellar-phase), 8 compounds (or 2 in the case of the hexadentate chelators), and ca. 30000 water molecules. The concentrations of the compounds were ca. $2 \times 10^{-3} \text{ M}$ and $9 \times 10^{-3} \text{ M}$ for the hexadentate and bidentate chelators, respectively. The simulations were conducted in the NPT ensemble and with the SLIPIID parameters^{36–38} adapted to the AMBER 12.0^{39,40} software (described in detail in the Supporting Information). The CUDA implementation was employed.^{41,42} Initially, the tested compounds were placed at an approximate distance of 5 Å of the bilayer model, to evaluate the tropism for interaction (defined as group A simulations). However, the simulations were also performed starting with the compounds docked at the surface of the bilayer (defined as group B). The area per lipid, and bilayer thickness quantities were validated and compared with experimental data (at 303 K)⁴³ (see Supporting Information, Table S2). A good correlation was found with an average deviation of ca. 2% for the DMPC bilayer. A minimization and a gradual heating of the systems were performed prior to the 40 ns simulations. A more detailed description of the simulation protocol, including

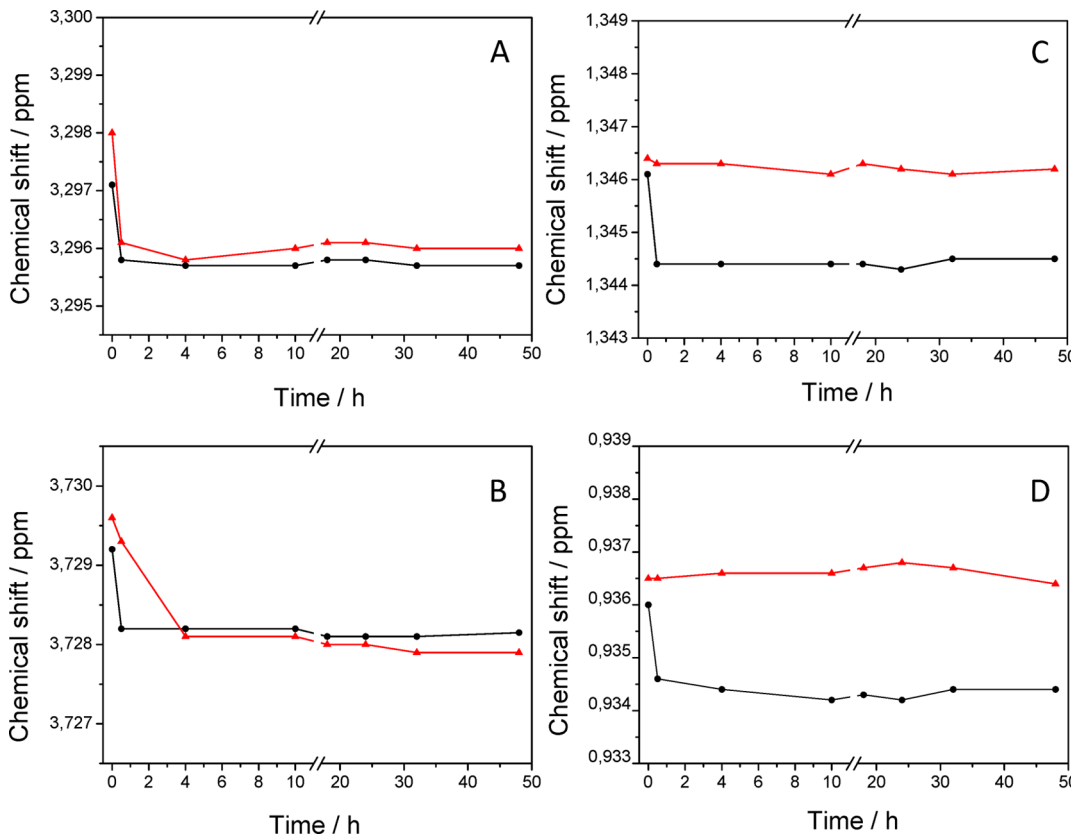


Figure 3. Variation along time of the chemical shift values of protons of different groups in the lipid structure in the presence of MRB7 (black circles) or MRB8 (red triangles): (A) $-\text{CH}_3$ choline (γ); (B) $-\text{NCH}_2$ choline (β); (C) $-\text{CH}_2$ acyl chain (4–13) and $-\text{CH}_3$ acyl chain (14).

algorithms^{44–47} and methods,^{48–53} is provided within the Supporting Information. The simulations amounted to a total of 400 ns simulation time –40 ns per case. The analyses were performed with the *cpptraj/ptraj* tool⁵⁴ and with the Visual Molecular Dynamics (VMD) program (version 1.9.1).⁵⁵ Distances of the compounds relative to membrane groups and the compounds' partition (CP) into the membrane was evaluated in these simulations, following the equation:

$$\text{CP} = \frac{\left[\sum_{i=1}^{\text{no.of compounds}} \text{dist}(\text{comp.} - \text{mem.}) \right]}{\text{simulation time} \times \text{no. of compounds}} \times 100, \text{dis} \\ t(\text{comp.} - \text{mem.}) \\ < \text{cutoff} \quad (1)$$

where the numerator represents the simulation time in which each compound is interacting with the bilayer; and the denominator, the simulation time multiplied by the total number of compounds in each MD run (8 for the bidentate and 2 for the hexadentate compounds). The numerator is defined by the cutoff that is related to the distance of each molecule to the bilayer plane defined by the nitrogen atoms from the choline groups of the DMPC phospholipids.

The conformations of the compounds in contact with the membrane, and type of molecular association were also considered.

Compounds:DC-SIGN Receptor Interaction. To evaluate the interaction of the compounds with the endocytic receptor DC-SIGN (PDBID: 1SL4 at 1.55 Å of resolution),⁷ molecular docking and subsequent MD simulations were performed.

The high-mannose binding receptor is bound with a tetrasaccharide composed by four mannose units (Man₄). All crystallographic water molecules and sugar residues were removed to obtain the unbound structure. Hydrogen atoms were added, taking into account all residues in their physiological protonation state. Furthermore, we set out to perform molecular docking with AutoDock Vina⁵⁶ for the Man₄ oligosaccharide and the following compounds: MRB5, MRB7, MRB8, and the pyridinone chelating unit (CHELu). The box was centered into Man₄ oligosaccharide and with a size of 21 × 22 × 19 Å. The values for exhaustiveness and modes were defined at 50. The $\Delta G_{\text{binding}}$ values of each solution were obtained from the knowledge-based scoring function of the AutoDock Vina program. The program VMD was used for visual inspection, analysis and preparation of the figures of the docking results.

To evaluate if the compounds maintain their molecular association with the tested receptors, MD simulations of 10 ns each were performed (a total of 50 ns). A detailed description of the MD simulation protocol is provided within the Supporting Information.

RESULTS AND DISCUSSION

NMR Spectroscopy. The affinity of MRB7 and MBR8 for the phospholipid bilayer of DMPC liposomes and the chelators permeation properties were estimated on the basis of the induced alterations of a number of NMR parameters, such as chemical shifts, line shape, spin–lattice relaxation time (T_1), and translational diffusion coefficient of the lipids and the liposomes. The analysis was focused on the variation of the NMR parameters of the lipid molecules since no signals of

MRB7 and MBR8 protons were detected for the concentration used (≈ 20 mM DMPC: ≈ 30 μM chelator). The NMR study was first carried out on “pure” DMPC liposome samples to fully characterize the aggregates and afterward on samples prepared by incubation of MRB7 or MBR8 with DMPC liposomes (DMPC_MRB7 and DPMC_MRB8 samples) thus allowing the analysis of changes, induced by the presence of compounds MRB7 or MBR8, on characteristic parameters of the NMR spectra of the phospholipid bilayer of DMPC liposomes. NMR spectral analysis was carried out in the time range from 30 min to 48 h after incubation of liposomes with MRB7 and MBR8.

A typical ^1H NMR spectrum of DMPC liposomes in D_2O at 310 K with the assignment of the characteristic proton resonances in the molecule is presented in Figure 2.

The chemical shift changes of the lipid resonances of protons ($-\text{CH}_3$ choline (γ), $-\text{NCH}_2$ choline (β), $-\text{CH}_2$ (4–13) and $-\text{CH}_3$, (14)) observed after adding of MRB7 and MBR8, for the time interval from 0.5 to 48 h are depicted in the graphics in Figure 3A–D. The chemical shift changes of the lipid resonances of protons of the glycerol framework, $-\text{OCH}_2$ (sn1, sn3), $-\text{OCH}$ (sn2), were also registered and are shown in Supporting Information, Figure S2A,B).

Upon 0.5 h of incubation of the liposomes with the chelators, the resonances of *N*-methyl (γ) and *N*-methylene (β) protons of the choline groups located at the liposome surface are upfield shifted relative to the samples of the “pure” liposomes in both DMPC_MRB7 and DPMC_MRB8 samples (Figure 3, parts A and B). These chemical shift changes show the empathy of both MRB7 and MBR8 molecules to interact with the hydrophilic surface of phospholipid bilayer. A significant drop is observed after 0.5 h upon incubation and the chemical shift value is not further altered in the time interval of the experiment. We believe that the electrostatic interactions between the local charges of the neutral MRB7 or MRB8 molecules and lipids at the lipid–water interface play a dominant role in the molecular association to liposomes.

The changes in the resonances of the terminal protons of the acyl chains $-\text{CH}_2$ (4–13) and $-\text{CH}_3$ (14) (Figure 3, parts C and D) provide the most important difference between the permeation ability of chelators MRB7 and MBR8. The addition of MRB7 to the DMPC vesicles induces significant upfield shift of the resonance signals of the methyl and methylene protons of the hydrophobic chain region of the phospholipid bilayer in contrast with the addition of MBR8 upon which no significant changes are observed in the chemical shifts of the protons $-\text{CH}_2$ (13) and $-\text{CH}_3$ (14). Again, a significant drop in the chemical shift value is observed after 0.5 h upon incubation and no further change was registered in the time interval of the experiment.

The chemical shift values of protons of the glycerol framework, $-\text{OCH}_2$ (sn1, sn3), $-\text{OCH}$ (sn2) suffered very small or no changes upon incubation of the liposomes with the chelators (Figure S2).

The chemical shift changes observed for the protons associated with the different functional groups of the phospholipid can be related with a different distribution and location of MRB7 and MBR8 in the phospholipid bilayer of DMPC. The results suggest that chelator MRB7 strongly interacts with the choline head groups at the surface of the liposome sphere and is able to permeate deeper and reach the center of hydrophobic area of the phospholipid bilayer as demonstrated by the significant perturbations of the proton resonances induced on the terminal protons of the acyl chains

located in that area. In contrast, MBR8 molecules strongly interact with the polar surface of liposomes and seem to be preferably trapped between the polar interface and ester groups of the lipid bilayer thus justifying the nonperturbation of the proton resonances belonging to the lipid acyl chains.

The above results obtained along a period of 48 h suggest a bimodal distribution of MRB7 in DMPC liposomes with some MRB7 molecules located at the choline and some at the lipid acyl chains region while most MBR8 molecules preferably occupy the surface of the liposome. Additionally, the induced chemical shift changes in ^1H NMR spectra of liposomes were found to occur in a shorter time interval in the presence of MRB7 than MBR8 and hence the results also suggest a stronger affinity of MRB7 to associate with the phospholipid bilayer of the DMPC liposomes.

The presence of *N*-diethyl groups in the xanthene structure and the thiourea link in the structure of MRB7, as opposed to *N*-dimethyl groups in the xanthene structure and an amide link in the structure of MBR8, seem to facilitate the affinity of MRB7 molecules to the liposome surface and their ability to penetrate deeper into the hydrophobic interior of lipid bilayer. No further changes in ^1H NMR spectra of (DMPC_MRB7 and DPMC_MRB8 were registered up to 48 h after incubation.

Diffusion NMR spectroscopy (DOSY)^{57,58} is particularly sensitive to structural and dynamical changes at molecular level and represents a powerful tool for studying the complex processes of the interaction between pharmacologically active compounds and cellular membranes and to predict pharmacokinetic properties for their efficacy. Herein, Diffusion NMR spectroscopy (^1H DOSY) was applied to further explore the interactions of MRB7 and MBR8 with DMPC liposomes and to evaluate the mechanisms of penetration and distribution of both compounds into the phospholipid bilayer of liposomes. The diffusion coefficient of DMPC liposomes in a presence of 30 μM of MRB7 or MBR8 were measured and compared with the corresponding values obtained for the “pure” liposomes. Time dependent alterations in the diffusion of liposomes were followed up to 48 h after incubation with MRB7 or MBR8. The diffusion coefficients (D) of liposomes in the samples studied were determined from the resonance signals of the *N*-methyl protons of the choline residues and scaled to the D value obtained for $\text{DMSO}-d_6$. Due to the typical spectral line broadening and severe overlap of signals in ^1H NMR spectra of liposomes, the resonance signals belonging to *N*-methyl protons of the associated with MRB7 or MBR8 lipids molecules could not be distinguished. This means that the D values defined will contain contribution from both the free and associated with MRB7 or MBR8 lipid molecules.

The D coefficients determined for the “pure” liposomes and after incubation with MRB7 or MBR8, for the time interval studied are presented in Figure 4.

The observed significant changes in the diffusion rate of liposomes shortly after mixing with MRB7 or MBR8 are an indication for the transfer of molecules of both compounds from the bulk water environment to the polar surface of liposomes and interaction with phospholipid bilayers. The results show that MRB7 has stronger effect on the liposomes diffusion than MBR8 (Figure 4), expressed by the stronger decrease of D coefficient of liposomes registered for DMPC_MRB7 samples for the time interval studied. In contrast, the D coefficient of the liposomes in DMPC-MRB8 samples was found to decrease immediately after adding of MBR8 but then to gradually increase to values even higher than those

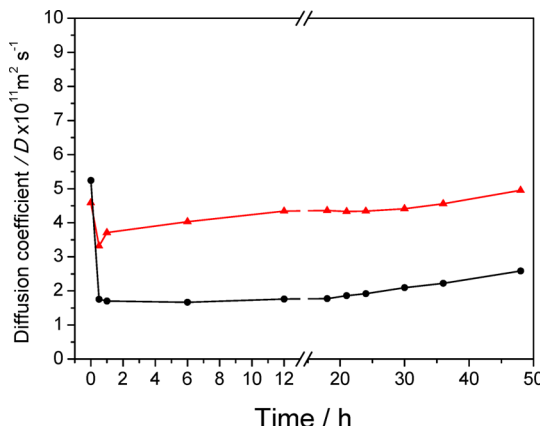


Figure 4. Diffusion coefficient ($D \times 10^{11} \text{ m}^2 \text{ s}^{-1}$) values obtained from $-\text{CH}_3$ choline (γ) protons in DMPC structure in the presence of MRB7 (black circles) or MRB8 (red triangles).

determined for the pure liposomes. The different diffusion behavior of liposomes in the presence of MRB7 and MRB8 was attributed to the different affinity of both compounds to associate and penetrate into the lipid bilayer of liposomes. This affinity is related to the specific structural characteristics of MRB7 and MRB8 discussed above. The significant slowdown of liposomes diffusion after mixing with MRB7 or MRB8 may be due to many factors such as changes in the shape, surface charges, mobility, disruption of well-organized structure of lipid bilayer.^{59,60} The stronger effect of MRB7 should be due to the distribution of MRB7 molecules at the liposomes surface as well as in the interior of lipid bilayer. The contribution of these two factors results in significant decrease of the diffusion of liposomes, which was found to be almost the same during a period of 36 h. The suggested above location of MRB8 between the polar interface and ester groups of lipid bilayer should mainly affect the outer curvature of the liposomes that could explain the weaker changes in liposomes diffusion. The observed fluctuation of the D coefficient could be due to exchange of MRB8 molecules between water and liposomes environment in the system.

Compounds: Membrane Interaction by MD Simulations. The tropism for a DMPC bilayer model was evaluated, considering all the tested compounds. The computational results will focus on the mode and the degree interaction with this computational model, which will be further related to the experimental results.

The initial position of the drugs, relative to the membrane was evaluated. We have started from the compounds, placed at a certain distance of the bilayer (ca. 5 Å). This granted us with means to evaluate the affinity for the bilayer, the water phase and among them. This is conceptually and biologically more realistic, rather than starting from an already “docked” assembly with the bilayer. However, the tested compounds were also placed at the surface of the bilayer assembly. Hence, limited intermolecular interactions (between the compounds) would be observed and desolvation energies would be lowered upon interaction, since the compounds were already docked at the surface.

For this analysis, we define the compounds’ partition (CP) as the amount of interaction of all the compounds, in each simulation, with the membrane model—defined by eq 1. Table 1 presents a summary of the % CP, for each compound.

Table 1. Characterization of the Interaction between the Listed Compounds and the DMPC Membrane Model through the Percentage of the Compounds’ Partition (%) CP) Quantity, Defined in Eq 1

group	compound ID	% CP
A	MRB5	55
	MRB7	16
	MRB8	14
	MRH7	0
	MRH7:Fe ³⁺	0
B	MRB5'	86
	MRB7'	93
	MRB8'	65
	MRH7'	79
	MRH7:Fe ³⁺	38

For DMPC, two groups of simulations were defined: group A, represented by the MD simulations starting with the compounds at ca. 5 Å of the membrane/water phase; and group B, starting with the same compounds close to the membrane phase.

Interestingly, for group A, we cannot observe a strong interaction of all the compounds with the membrane model. In fact, the drugs that have shown higher antimycobacterial activity—MRB7 and MRB8—do have the lowest % CP; or even show no higher affinity for the membrane, as in the case of MRH7. This lower interaction with the membrane model, and in the case of the bidentate ligands, can be attributed to the high intermolecular association observed for these molecules. This has been described experimentally, for rhodamine-related compounds, which is part of the composition of MRB7 and MRB8.^{61,62} Since these compounds were initially placed farther from the bilayer, they have showed a tendency to agglomerate (see Supporting Information, Figure S3), and to neglect the interaction with the bilayer. This behavior is also probably related to the short simulation times conducted, and we expect that extended simulations could improve the interaction profile for the compounds, when considering the simulations in which the molecules were placed further from the membrane. Nonetheless, for one of the 8 molecules of each chelator, the interaction profile with the bilayer is incredibly strong (see Supporting Information, Figure S3).

The absence of interaction of the hexadentate compounds, could be related to the strong intramolecular interactions observed, namely through $\pi-\pi$ stacking. This granted the compounds a bulky conformation, which could hamper the interaction with the DMPC bilayer in the tested time scales.

Bidentate Chelators. A detailed analysis on the mode of interaction of each bidentate molecule was further considered. For group A, MRB5 presented the highest number of interacting compounds (Table 1, group A). These, however, seem to remain more retained in the polar region of the membrane. This could be related partly to the results connected with the different mechanisms of uptake and subcellular distribution detected for the compounds.³

Despite the lower interaction of the aggregated MRB7 and MRB8 compounds, their aggregates remain also at the surface of the bilayer, which can be indicative of the tropism for the lipidic phases. To observe if the initial position was indeed the factor, which was reducing the number of interacting compounds, a second MD simulation was performed for MRB5, MRB7 and MRB8 (defined as MRB5', MRB7', and

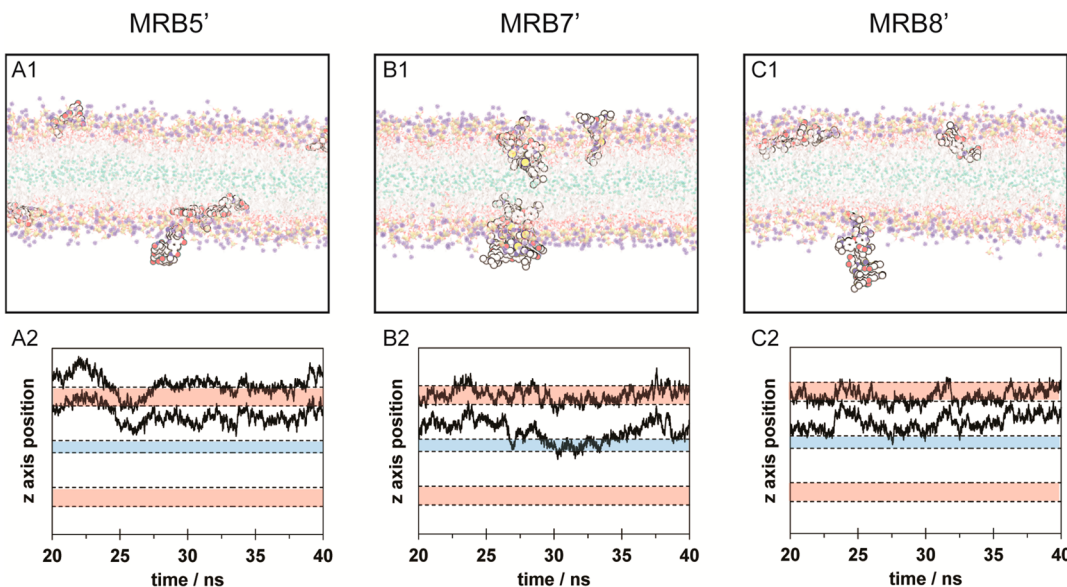


Figure 5. Graphical representation of the interaction of the tested bidentate compounds—MRB5' (A1), MRB7' (B1) and MRB8' (C1)—with the DMPC bilayer model. The second panel of each category (A2, B2 and C2) represents the position of the compounds relative to the membrane's plane, considering the minimum and maximum z coordinates of an illustrative compound. In the graphical charts, in red we have the polar region of the membrane; and in blue the nonpolar region comprised of the terminal methyl groups of the phospholipids' acyl chains.

MRB8'). Here we have placed the compounds closer to the surface of the membrane. Indeed, the interaction profile increased for these simulations (Table 1, group B). The results also suggest that MRB7' seems to have the higher insertion and residence time in the hydrophobic region of the bilayer, in comparison with MRB5' and MRB8' (see Figure 5). This is consistent with the NMR results, which show an NMR shift for the MRB7 compound comprising the terminal carbon atoms of the acyl chains. MRB8' also interacts with the hydrophobic phase, but it fluctuates more between regions (see Figure 5C), and does not seem to go as deep as the MRB7' compound; nor the number of interacting compounds is comparable with MRB7' (see Table 1, group B).

We have observed also the type of interaction with the bilayer. In Figure 6, we can see the molecular association in the bilayer, and it seems that the compounds are able to indiscriminately interact by the rhodamine or chelating group. However, it appears that only through the rhodamine group they are able to penetrate deeper in the bilayer. For compounds MRB7 and MRB8 the drugs can go as deep in the bilayer as to surpass the plane defined by the ester oxygen atoms (these represent the end of the polar region, and the beginning of the nonpolar one).

This is an expected result, since the substituted amine group, and the highly hydrophobic rings, are more prone to interact with hydrophobic membrane regions. In contrast, the MRB5' compound is more polar in its fluorescent unit and consequently it becomes more deposited in the hydrophilic portion of the bilayer.

Hexadentate Chelator. On the hexadentate chelator (MRH7), we observe high intramolecular interactions, mainly through $\pi-\pi$ stacking (see Figure 7, panel A). This could grant the molecules a bulkier assembly, which could prevent their interaction with the bilayer in the tested time frame. To further test our hypothesis, as in the bidentate cases, the MD simulation was repeated for MRH7. The compounds were placed closer to the surface of the bilayer (MRH7'). We observe that these compounds are able to interact with the

bilayer, but at a more superficial level than the analogous bidentate ligand (MRB7') (see Figure 7, panel B). In addition, the two subjects of this simulation assemble, interacted with the bilayer through the polar chelating units, which could prevent their higher insertion in the bilayer. Previously, experimental results have characterized the interaction of this compound in experiments with liposomes.³ However, these results are not unexpected. In experimental setups the conformational sampling is larger, due to the experimental time lengths (hours and minutes).

Iron(III) Coordinated to MRH7 Compound. The MRH7 compound was additionally bound with iron. We see that in group A simulations, the compounds did not interact with the bilayer in the tested time-length (Table 1, group A). As for group B simulations (Table 1, group B), some degree of insertion is detected. When comparing with the noncoordinated compound, we see no relevant differences, despite the fact that in Table 1, group B, a lower % CP is observed for MRH7:Fe³⁺. This could be related to the reduced number of molecules in the simulation box (only 2 molecules).

In the last portion of the MD simulation, MRH7:Fe³⁺ seems to become more inserted in the bilayer, through the chelating unit (Figure 7, panel C). We believe that the protection of the polar atoms in the chelating unit, mediated by the inclusion of iron(III), could be the cause.

Compounds: DC-SIGN Receptor Interaction. The biological activity results previously obtained showed that the fluorescent chelators derived from rhodamine (MRB7, MRH7, MRB8, and MRH8) have a significantly higher antimicrobial activity than those derived from fluorescein (MRH5).² Confocal microscopy studies showed that all the chelators have access to the macrophage but their distribution in the cell is different and chelators do not reach the same compartments within the cell.³ The dissimilar cellular distribution has been related with the different affinity of chelators to DMPC liposomes, which was investigated by fluorescence spectroscopy.³

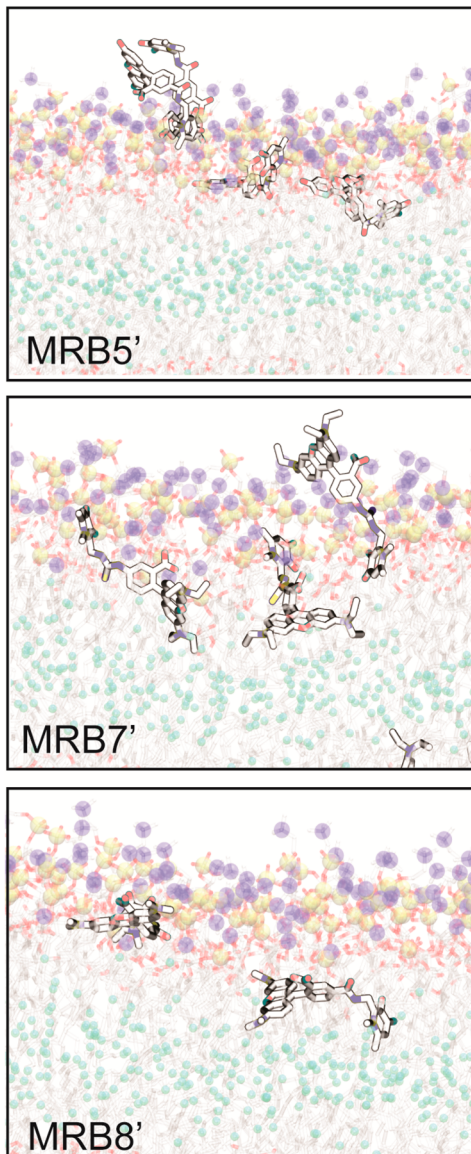


Figure 6. Representative snapshot of the MRB5', MRB7', and MRB8' mode of interaction with the DMPC bilayer. The polar region is represented by blue and orange spheres, and in red sticks; the nonpolar region by light gray sticks and green spheres.

In this work we observed that there is an apparent higher interaction of all these compounds with lipidic phases (bilayer insertion depth ordered: MRB7 > MRB8 > MRB5). Several efforts have been done to understand the transport of these compounds through the bilayer, because it is very unlikely that ionic large molecules would cross the bilayer through diffusion. It has been proposed in the literature that rhodamine123 could cross cells through protein-mediated mechanisms in Caco-2 cells.⁶³ Hence, we have tested a possible transport hypothesis through docking and MD calculations, taking into consideration an endocytic receptor (DC-SIGN). This choice is supported by the rhodamine's capacity for marking endosomes and lysosomes, in some cell types.⁶⁴ DC-SIGN belongs to C-type lectin receptors and is responsible for pathogen recognition and signaling. The DC-SIGN receptors mediate both endocytosis and phagocytosis that facilitate clearance of compounds and this receptor binds and recognizes the compounds through calcium cations. In general, Ca^{2+} is

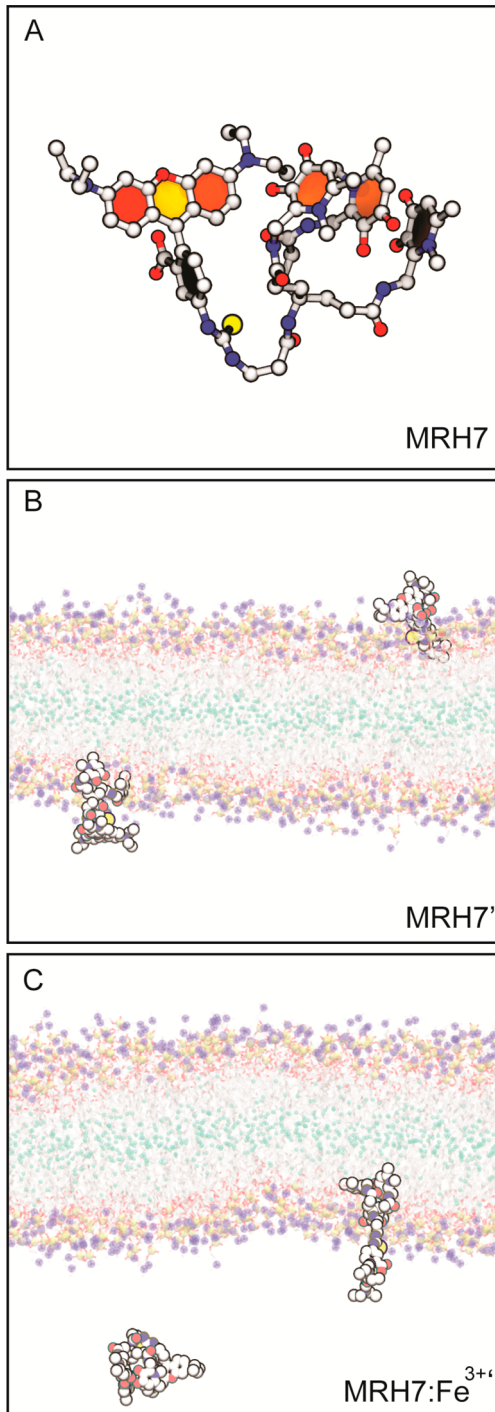


Figure 7. Representation of the intramolecular interactions observed in the MRH7 compound (panel A). Molecular representation of the interaction of the hexadentate compounds (MRH7' and MRH7:Fe^{3+}) with the DMPC membrane model (panels B and C).

centered in an eight-coordinated cubic geometry⁶⁵ and strongly prefers oxygen over nitrogen or sulfur ligands. The Ca^{2+} ion, which is present in the studied DC-SIGN receptor structure shows an oxygen atom coordination sphere provided by six different ligands: Glu95, Asn97, bidentate Glu102, Asn113, Asp114, and the mannose unit from Man_4 oligosaccharide (in a bidentate mode). Initially, we have performed docking of the Man_4 oligosaccharide to the receptor's binding site, in order to validate the docking protocol. Figure S4 shows the super-

imposition of the crystallographic and docked structures. It was observed that the docked mannose residue directly bound to calcium adopts a very similar arrangement to the crystallographic one. This supports the high performance of the docking software in predicting the binding mode of ligands into the receptor's binding site. The $\Delta G_{\text{binding}}$ value obtained for the best ranked Man_4 solution was $-7.4 \text{ kcal mol}^{-1}$. Subsequently, we have applied the same docking parameters to evaluate the possible interaction of MRB5, MRB7, and MRB8 compounds with this receptor. Table 2 shows the binding free energy values

Table 2. Binding Free Energy Values Obtained for the First Top-Ranked Solutions of Each Docking Process (Man_4 or Chelating Molecules)

compound	$\Delta G_{\text{binding}}/\text{kcal}\cdot\text{mol}^{-1}$
Man_4	-7.4
MRB5	-7.2
MRB7	-7.0
MRB8	-6.9
CHELu	-4.2

obtained for the first top-ranked solution of each docking process (Man_4 and chelating molecules). When comparing all the $\Delta G_{\text{binding}}$ values, we can observe that all chelating compounds show similar affinities to the receptor (ranging from 6.9 to $7.2 \text{ kcal}\cdot\text{mol}^{-1}$) and close to the natural substrate Man_4 ($-7.4 \text{ kcal}\cdot\text{mol}^{-1}$). The chelating unit—CHELu—however, shows a lower free energy value that can prelude a weaker interaction with DC-SIGN. To test the affinity for the receptor's binding site, all of these were considered for further MD simulations. During 10 ns, the position of the ligand relative to the receptor was evaluated. It was observed that the natural substrate for the receptor— Man_4 molecule—remains coordinated to calcium during the whole MD simulation (see Supporting Information, Figure S5).

The behavior of the compounds binding to the receptor was then evaluated by also performing 10 ns simulations using as a starting geometry the structures from the docking protocol. The interaction of MRB5, MRB7, and CHELu with Ca^{2+} occurs by the chelating unit, while the MRB8 interacts by the carboxylate group. In Figure 8 we present a graphical representation of the average structures of the first and last nanosecond of each MD simulation. The receptor backbone and chelating compound's root-mean-square deviation (RMSd) values, as well as the closest distance to the calcium ion, were obtained and are represented in Figure S5. The receptor's RMSd values ranged between 1.0 and 2.0 \AA , indicating that the overall folding is stable and the equilibration of each system was achieved.

Similarly to the sugar, it was observed that the MRB7 and MRB8 are always bound to the receptor, showing the closest distances to calcium—an average of $2.62 \pm 0.08 \text{ \AA}$ in the last nanosecond. In addition to the strong electrostatic interaction established with the Ca^{2+} ion, there is a short H-bond between Arg93 and the rhodamine group of both compounds. Hydrophobic T-shaped stacking interactions and van der Waals contacts between Phe61 and Val99 residues to the aromatic rings of these chelating compounds were also observed. Regarding the MRB5 compound, in the beginning of the MD simulation, this compound interacts weakly with the receptor but, after ca. 6 ns , a small conformational arrangement occurred and MRB5 starts to strongly interact with the

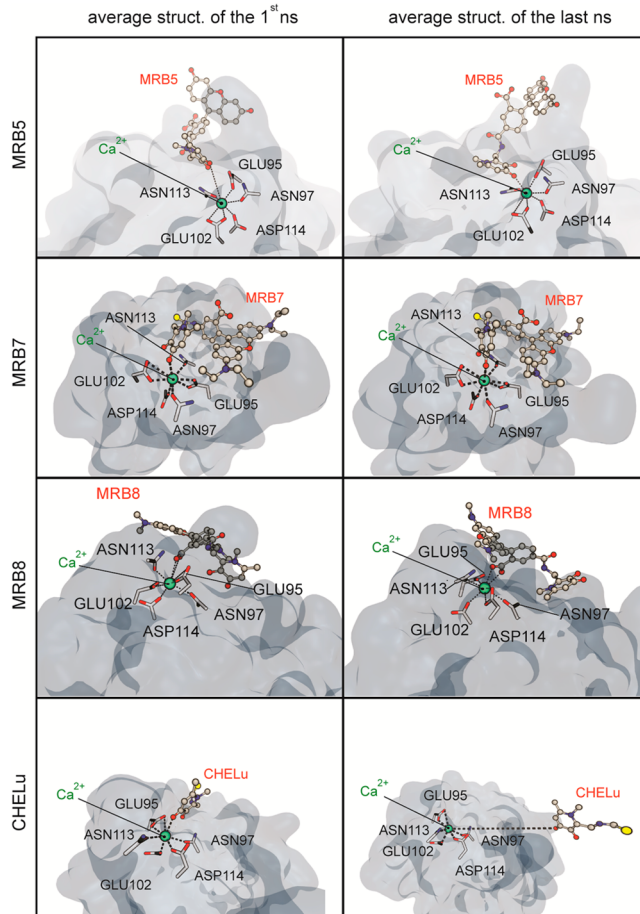


Figure 8. Average structures of the first and last nanosecond of each MD simulation of the chelating compounds.

receptor, showing an average distance to calcium of $2.97 \pm 0.50 \text{ \AA}$ in the last nanosecond.

Since the main binding mode of these compounds to the calcium ion of the receptor occurs through the chelating ring, the CHELu compound was also studied in order to evaluate the role of the rhodamine unit for the binding. Analyzing the MD simulation, it was observed that initially, this molecule interacts with the receptor. However, after 4 ns CHELu begins to detach from the receptor. This data suggests that the presence of the xanthene rings present in the rhodamine/fluorescein groups of these chelating compounds is fundamental for their binding to this transmembrane receptor. Furthermore, taking into account the average distance between the compounds and calcium, it was also proposed that the binding of MRB7 and MRB8 compounds to the receptor is stronger than for the MRB5. Considering all these MD results, we propose that the entrance of these large chelating molecules to the interior of macrophages may be mediated by interaction with DC-SIGN and mannose transmembrane receptors. Their strong binding induces endocytosis, and furthermore, the acidic pH induces conformational rearrangements of the receptor, releasing the compounds.

CONCLUSIONS

The NMR and MD simulation results reported here substantiate our premise that a strong affinity for lipid bilayers is crucial for the biological activity.³ The results show that chelators interact with the lipid phases at different levels of the

bilayer and that the interaction seems to be strengthened for the rhodamine labeled compounds, in particular for the compounds that contain ethyl groups and a thiourea linkage (MRB7 and MRH7) which are those exhibiting the highest biological activity.^{1,2} Both NMR and MD simulation results show that compound MRB7 not only interacts strongly with bilayer phases but this interaction comprises the hydrophobic region of the membrane models employed. We also observe that this interaction is far stronger or superior than that of the related MRB5 and MRB8 compounds. The diffusion coefficient values obtained by NMR for MRB7 and MRB8 clearly show that MRB7 molecules must distribute at the liposomes surface as well as in the interior of lipid bilayer while MRB8 is likely to be mostly retained at the surface mainly affecting the outer curvature of the liposomes.

The molecular docking and MD simulations performed for the potential interaction of the chelators with DC-SIGN receptors, which are present in dendritic cells, provide valuable additional information regarding the cellular uptake of these compounds. The results show that the chelators interact with the DC-SIGN receptor and that the fluorophore fragment of the molecular framework is essential for an efficient binding, thus providing a possible explanation for the inactivity of the 3,4-HPO chelating unit in the *M. avium* infection model.² Among the fluorescent chelators, the compound that contains ethyl substituents on the amino groups of the xanthene ring and a thiourea link (MRB7) is the one that exhibits a stronger binding to this receptor. The compounds MRB7 and MRH7 are those that exhibit a stronger biological activity. This result is not proof that the mechanism of entrance of these compounds is set by these receptors and future experiments will focus on the study of such mechanism of internalization.

The studies regarding the interaction of the chelators with the DC-SIGN receptor are the first step of the study regarding the mechanism of entrance of these compounds in cells that harbor mycobacteria.

The present results reinforce the hypothesis³ that a differential interaction of fluorescein and rhodamine-labeled chelators with membranes is determinant for their differential cellular uptake and distribution. Moreover, considering the set of rhodamine-derived chelators, the present results provide evidence that different substituents in the rhodamine framework tune the chelators' capacity to permeate and progress through biological membranes.

■ ASSOCIATED CONTENT

Supporting Information

Detailed molecular dynamics simulation protocol, specifying additional information in regards to the simulation conditions, parameter files for each of the tested compounds, complementary results, on the structural validation of the membrane models, and supporting results, on the interaction profile between the compounds and the bilayer models used. This material is available free of charge via the Internet at <http://pubs.acs.org>.

■ AUTHOR INFORMATION

Corresponding Authors

*E-mail: mcrangel@fc.up.pt (M.R.).

*E-mail: mjramos@fc.up.pt (M.J.R.).

Author Contributions

[§](J.T.S.C., T.M., N.F.B., G.I.) These authors contributed the same.

Notes

The authors declare no competing financial interest.

■ ACKNOWLEDGMENTS

This work received financial support from the European Union (FEDER funds through COMPETE) and National Funds (FCT, Fundação para a Ciência e Tecnologia) through Project Pest-C/EQB/LA0006/2013. The work also received financial support from the European Union (FEDER funds) under the framework of QREN through Project NORTE-07-0124-FEDER-000066. The Bruker Avance III 600 HD spectrometer was purchased under the framework of QREN, through Project NORTE-07-0162-FEDER-000048, and is part of the Portuguese NMR Network created with support of the Portuguese Foundation for Science and Technology through Contract REDE/1517/RMN/2005, with funds from POCI 2010 (FEDER) and FCT. To all financing sources, the authors are greatly indebted. J.T.S.C. and T.M. thank the FCT for their Ph.D. grants (SFRH/BD/87434/2012 and SFRH/BD/79874/2011, respectively).

■ REFERENCES

- (1) Moniz, T.; Nunes, A.; Silva, A. M. G.; Queirós, C.; Ivanova, G.; Gomes, M. S.; Rangel, M. Rhodamine Labeling of 3-Hydroxy-4-Pyridinone Iron Chelators Is an Important Contribution to Target Mycobacterium Avium Infection. *J. Inorg. Biochem.* **2013**, *121* (0), 156–166.
- (2) Fernandes, S. S.; Nunes, A.; Gomes, A. R.; de Castro, B.; Hider, R. C.; Rangel, M.; Appelberg, R.; Gomes, M. S. Identification of a New Hexadentate Iron Chelator Capable of Restricting the Intramacrophagic Growth of Mycobacterium Avium. *Microb. Infect.* **2010**, *12* (4), 287–294.
- (3) Nunes, A.; Podinovskaya, M.; Leite, A.; Gameiro, P.; Zhou, T.; Ma, Y.; Kong, X.; Schaible, U.; Hider, R.; Rangel, M. Fluorescent 3-Hydroxy-4-Pyridinone Hexadentate Iron Chelators: Intracellular Distribution and the Relevance to Antimycobacterial Properties. *JBIC, J. Biol. Inorg. Chem.* **2010**, *15* (6), 861–877.
- (4) Bucki, R.; Janmey, P. A. Interaction of the Gelsolin-Derived Antibacterial Pbp 10 Peptide with Lipid Bilayers and Cell Membranes. *Antimicrob. Agents Chemother.* **2006**, *50* (9), 2932–2940.
- (5) Bucki, R.; Pastore, J. J.; Randhawa, P.; Vagners, R.; Weiner, D. J.; Janmey, P. A. Antibacterial Activities of Rhodamine B-Conjugated Gelsolin-Derived Peptides Compared to Those of the Antimicrobial Peptides Cathelicidin LL37, Magainin II, and Melittin. *Antimicrob. Agents Chemother.* **2004**, *48* (5), 1526–1533.
- (6) Feinberg, H.; Torgerson, D.; Drickamer, K.; Weis, W. I. Mechanism of Ph-Dependent N-Acetylgalactosamine Binding by a Functional Mimic of the Hepatocyte Asialoglycoprotein Receptor. *J. Biol. Chem.* **2000**, *275*, 35176–35184.
- (7) Guo, Y.; Feinberg, H.; Conroy, E.; Mitchell, D. A.; Alvarez, R.; Blixt, O.; Taylor, M. E.; Weis, W. I.; Drickamer, K. Structural Basis for Distinct Ligand-Binding and Targeting Properties of the Receptors Dc-Sign and Dc-Signr. *Nat. Struct. Mol. Biol.* **2004**, *11* (7), 591–598.
- (8) Hwang, T.-L.; Shaka, A. J. Water Suppression That Works—Excitation Sculpting Using Arbitrary Waveforms and Pulse Field Gradients. *J. Magn. Reson., Ser. A* **1995**, *112*, 275–279.
- (9) Wu, D. H.; Chen, A. D.; Johnson, C. S. An Improved Diffusion-Ordered Spectroscopy Experiment Incorporating Bipolar-Gradient Pulses. *J. Magn. Reson., Ser. A* **1995**, *115* (2), 260–264.
- (10) Bayly, C. I.; Cieplak, P.; Cornell, W.; Kollman, P. A. A Well-Behaved Electrostatic Potential Based Method Using Charge Restraints for Deriving Atomic Charges: The Resp Model. *J. Phys. Chem.* **1993**, *97* (40), 10269–10280.

- (11) Brillouin, L. *Les Champs Self-Consistents De Hartree Et De Fock*; Hermann: Paris, 1934.
- (12) Fock, V. Nähierungsmethode Zur Lösung Des Quantenmechanischen Mehrkörperproblems. *Z. Phys.* **1930**, *61*, 126–148.
- (13) Hartree, D. R.; Hartree, W. Self-Consistent Field, with Exchange, for Beryllium. *Proc. R. Soc. London, Ser. A: Math.Phys. Sci.* **1935**, *150* (869), 9–33.
- (14) Roothaan, C. C. J. New Developments in Molecular Orbital Theory. *Rev. Mod. Phys.* **1951**, *23* (2), 69–89.
- (15) Slater, J. C. Note on Hartree's Method. *Phys. Rev.* **1930**, *35* (2), 210–211.
- (16) Slater, J. C. A Simplification of the Hartree-Fock Method. *Phys. Rev.* **1951**, *81* (3), 385–390.
- (17) Francis, M. M.; Pietro, W. J.; Hehre, W. J.; Binkley, J. S.; Gordon, M. S.; Defrees, D. J.; Pople, J. A. Self-Consistent Molecular-Orbital Methods 0.23. A Polarization-Type Basis Set for 2nd-Row Elements. *J. Chem. Phys.* **1982**, *77* (7), 3654–3665.
- (18) Ditchfield, R.; Hehre, W. J.; Pople, J. A. Self-Consistent Molecular-Orbital Methods. IX. An Extended Gaussian-Type Basis for Molecular-Orbital Studies of Organic Molecules. *J. Chem. Phys.* **1971**, *54* (2), 724–728.
- (19) Wang, J.; Wolf, R. M.; Caldwell, J. W.; Kollman, P. A.; Case, D. A. Development and Testing of a General Amber Force Field. *J. Comput. Chem.* **2004**, *25* (9), 1157–1174.
- (20) Becke, A. D. Density-Functional Thermochemistry. III. The Role of Exact Exchange. *J. Chem. Phys.* **1993**, *98* (7), 5648–5652.
- (21) Lee, C.; Yang, W.; Parr, R. G. Development of the Colle-Salvetti Correlation-Energy Formula into a Functional of the Electron Density. *Phys. Rev. B* **1988**, *37* (2), 785–789.
- (22) Vosko, S. H.; Wilk, L.; Nusair, M. Accurate Spin-Dependent Electron Liquid Correlation Energies for Local Spin Density Calculations: A Critical Analysis. *Can. J. Phys.* **1980**, *58* (8), 1200–1211.
- (23) Stephens, P. J.; Devlin, F. J.; Chabalowski, C. F.; Frisch, M. J. Ab Initio Calculation of Vibrational Absorption and Circular Dichroism Spectra Using Density Functional Force Fields. *J. Phys. Chem.* **1994**, *98* (45), 11623–11627.
- (24) Neves, R. P. P.; Sousa, S. F.; Fernandes, P. A.; Ramos, M. J. Parameters for Molecular Dynamics Simulations of Manganese-Containing Metalloproteins. *J. Chem. Theory Comput.* **2013**, *9* (6), 2718–2732.
- (25) Sousa, S.; Fernandes, P.; Ramos, M. Effective Tailor-Made Force Field Parameterization of the Several Zn Coordination Environments in the Puzzling Ftase Enzyme: Opening the Door to the Full Understanding of Its Elusive Catalytic Mechanism. *Theor. Chem. Acc.* **2007**, *117* (1), 171–181.
- (26) Dolg, M.; Wedig, U.; Stoll, H.; Preuss, H. Energy-Adjusted Ab initio Pseudopotentials for the First Row Transition Elements. *J. Chem. Phys.* **1987**, *86* (2), 866–872.
- (27) McLean, A. D.; Chandler, G. S. Contracted Gaussian Basis Sets for Molecular Calculations. I. Second Row Atoms, $Z = 11–18$. *J. Chem. Phys.* **1980**, *72* (10), 5639–5648.
- (28) Krishnan, R.; Binkley, J. S.; Seeger, R.; Pople, J. A. Self-Consistent Molecular Orbital Methods. XX. A Basis Set for Correlated Wave Functions. *J. Chem. Phys.* **1980**, *72* (1), 650–654.
- (29) Roos, B.; Veillard, A.; Vinot, G. Gaussian Basis Sets for Molecular Wavefunctions Containing Third-Row Atoms. *Theor. Chim. Acta* **1971**, *20* (1), 1–11.
- (30) Hay, P. J. Gaussian Basis Sets for Molecular Calculations. The Representation of 3d Orbitals in Transition-Metal Atoms. *J. Chem. Phys.* **1977**, *66* (10), 4377–4384.
- (31) Raghavachari, K.; Trucks, G. W. Highly Correlated Systems. Excitation Energies of First Row Transition Metals Sc–Cu. *J. Chem. Phys.* **1989**, *91* (2), 1062–1065.
- (32) Clark, T.; Chandrasekhar, J.; Spitznagel, G. W.; Schleyer, P. V. R. Efficient Diffuse Function-Augmented Basis Sets for Anion Calculations. III. The 3-21+G Basis Set for First-Row Elements, Li–F. *J. Comput. Chem.* **1983**, *4* (3), 294–301.
- (33) Frisch, M. J.; Pople, J. A.; Binkley, J. S. Self-Consistent Molecular Orbital Methods 25. Supplementary Functions for Gaussian Basis Sets. *J. Chem. Phys.* **1984**, *80* (7), 3265–3269.
- (34) Batsanov, S. S. Van Der Waals Radii of Elements. *Inorg. Mater.* **2001**, *37* (9), 871–885.
- (35) Jorgensen, W. L.; Chandrasekhar, J.; Madura, J. D.; Impey, R. W.; Klein, M. L. Comparison of Simple Potential Functions for Simulating Liquid Water. *J. Chem. Phys.* **1983**, *79* (2), 926–935.
- (36) Jämbeck, J. P. M.; Lyubartsev, A. P. Derivation and Systematic Validation of a Refined All-Atom Force Field for Phosphatidylcholine Lipids. *J. Phys. Chem. B* **2012**, *116* (10), 3164–3179.
- (37) Jämbeck, J. P. M.; Lyubartsev, A. P. An Extension and Further Validation of an All-Atomistic Force Field for Biological Membranes. *J. Chem. Theory Comput.* **2012**, *8* (8), 2938–2948.
- (38) Jämbeck, J. P. M.; Lyubartsev, A. P. Another Piece of the Membrane Puzzle: Extending Slipids Further. *J. Chem. Theory Comput.* **2012**, *9* (1), 774–784.
- (39) Case, D. A.; Babin, V.; Berryman, J. T.; Betz, R. M.; Cai, Q.; Cerutti, D. S.; Cheatham, T. E., III; Darden, T. A.; Duke, R. E.; Gohlke, H.; et al. *Amber 12*; University of California: San Francisco, CA, 2012.
- (40) Salomon-Ferrer, R.; Case, D. A.; Walker, R. C. An Overview of the Amber Biomolecular Simulation Package. *WIREs Comput. Mol. Sci.* **2013**, *3* (2), 198–210.
- (41) Götz, A. W.; Williamson, M. J.; Xu, D.; Poole, D.; Le Grand, S.; Walker, R. C. Routine Microsecond Molecular Dynamics Simulations with Amber on Gpus. I. Generalized Born. *J. Chem. Theory Comput.* **2012**, *8* (5), 1542–1555.
- (42) Le Grand, S.; Götz, A. W.; Walker, R. C. Spfp: Speed without Compromise—a Mixed Precision Model for Gpu Accelerated Molecular Dynamics Simulations. *Comput. Phys. Commun.* **2013**, *184* (2), 374–380.
- (43) Kucera, N.; Liu, Y. F.; Chu, N. J.; Petrache, H. I.; Tristram-Nagle, S.; Nagle, J. F. Structure of Fully Hydrated Fluid Phase Dmpc and Dlpc Lipid Bilayers Using X-Ray Scattering from Oriented Multilamellar Arrays and from Large Unilamellar Vesicles. *Biophys. J.* **2005**, *88* (1), 245a–245a.
- (44) Ryckaert, J.-P.; Cicotti, G.; Berendsen, H. J. C. Numerical Integration of the Cartesian Equations of Motion of a System with Constraints: Molecular Dynamics of N-Alkanes. *J. Comput. Phys.* **1977**, *23* (3), 327–341.
- (45) Pastor, R. W.; Brooks, B. R.; Szabo, A. An Analysis of the Accuracy of Langevin and Molecular Dynamics Algorithms. *Mol. Phys.* **1988**, *65* (6), 1409–1419.
- (46) Loncharich, R. J.; Brooks, B. R.; Pastor, R. W. Langevin Dynamics of Peptides - the Frictional Dependence of Isomerization Rates of N-Acetylalanyl-N'-Methylamide. *Biopolymers* **1992**, *32* (5), 523–535.
- (47) Grubmuller, H.; Heller, H.; Windemuth, A.; Schulten, K. Generalized Verlet Algorithm for Efficient Molecular Dynamics Simulations with Long-Range Interactions. *Mol. Simulat.* **1991**, *6*, 121–142.
- (48) Salomon-Ferrer, R.; Götz, A. W.; Poole, D.; Le Grand, S.; Walker, R. C. Routine Microsecond Molecular Dynamics Simulations with Amber on Gpus. 2. Explicit Solvent Particle Mesh Ewald. *J. Chem. Theory Comput.* **2013**, *9* (9), 3878–3888.
- (49) Berendsen, H. J. C.; Postma, J. P. M.; van Gunsteren, W. F.; DiNola, A.; Haak, J. R. Molecular Dynamics with Coupling to an External Bath. *J. Chem. Phys.* **1984**, *81* (8), 3684–3690.
- (50) Darden, T.; York, D.; Pedersen, L. Particle Mesh Ewald: An N Log(N) Method for Ewald Sums in Large Systems. *J. Chem. Phys.* **1993**, *98* (12), 10089–10092.
- (51) Essmann, U.; Perera, L.; Berkowitz, M. L.; Darden, T.; Lee, H.; Pedersen, L. G. A Smooth Particle Mesh Ewald Method. *J. Chem. Phys.* **1995**, *103* (19), 8577–8593.
- (52) Crowley, M.; Darden, T.; Cheatham, T., III; Deerfield, D., II Adventures in Improving the Scaling and Accuracy of a Parallel Molecular Dynamics Program. *J. Supercomput.* **1997**, *11* (3), 255–278.

- (53) Martínez, L.; Andrade, R.; Birgin, E. G.; Martínez, J. M. Packmol: A Package for Building Initial Configurations for Molecular Dynamics Simulations. *J. Comput. Chem.* **2009**, *30* (13), 2157–2164.
- (54) Roe, D. R.; Cheatham, T. E. PTRAJ and Cpptraj: Software for Processing and Analysis of Molecular Dynamics Trajectory Data. *J. Chem. Theory Comput.* **2013**, *9* (7), 3084–3095.
- (55) Humphrey, W.; Dalke, A.; Schulter, K. VMD: Visual Molecular Dynamics. *J. Mol. Graphics* **1996**, *14* (1), 33–38.
- (56) Trott, O.; Olson, A. J. Autodock Vina: Improving the Speed and Accuracy of Docking with a New Scoring Function, Efficient Optimization, and Multithreading. *J. Comput. Chem.* **2010**, *31* (2), 455–461.
- (57) Brand, T.; Cabrita, E. J.; Berger, S. Intermolecular Interaction as Investigated by NMR and Diffusion Studies. *Prog. Nucl. Magn. Reson. Spectrosc.* **2005**, *46* (4), 159–196.
- (58) Cohen, Y.; Avram, L.; Frish, L. Diffusion NMR Spectroscopy in Supramolecular and Combinatorial Chemistry: An Old Parameter—New Insights. *Angew. Chem., Int. Ed.* **2005**, *44* (4), 520–554.
- (59) Seddon, A. M.; Casey, D.; Law, R. V.; Gee, A.; Templer, R. H.; Ces, O. Drug Interactions with Lipid Membranes. *Chem. Soc. Rev.* **2009**, *38* (9), 2509–2519.
- (60) Schreier, S.; Malheiros, S. V. P.; de Paula, E. Surface Active Drugs: Self-Association and Interaction with Membranes and Surfactants. Physicochemical and Biological Aspects. *Biochim. Biophys. Acta (BBA)—Biomembranes* **2000**, *1508* (1–2), 210–234.
- (61) Moreno-Villalada, I.; Jofré, M.; Miranda, V.; González, R.; Sotelo, T.; Hess, S.; Rivas, B. L. pH Dependence of the Interaction between Rhodamine B and the Water-Soluble Poly(Sodium 4-Styrenesulfonate). *J. Phys. Chem. B* **2006**, *110* (24), 11809–11812.
- (62) Xiangying, S.; Bin, L.; Ying, Z. Rhodamine B Aggregation in Self-Assembled Multilayers Induced by Polyelectrolyte and Interfacial Fluorescence Recognition for DNA. *Talanta* **2011**, *85* (2), 1187–1192.
- (63) Troutman, M. D.; Thakker, D. R. Rhodamine 123 Requires Carrier-Mediated Influx for Its Activity as a P-Glycoprotein Substrate in Caco-2 Cells. *Pharm. Res.* **2003**, *20* (8), 1192–1199.
- (64) VonSteyern, F. V.; Josefsson, J. O.; Tagerud, S. Rhodamine B, a Fluorescent Probe for Acidic Organelles in Denervated Skeletal Muscle. *J. Histochem. Cytochem.* **1996**, *44* (3), 267–274.
- (65) Bertini, I.; Gray, H. B.; Lippard, S. J.; Valentine, J. S.; Forsén, S.; Kördel, J. Calcium in Biological Systems. In *Bioinorganic Chemistry*; University Science Books: Mill Valley, CA, 1994; pp 107–166.